

Article

Prediction and Experimental Study of Tire Slip Rate Based on Chassis Sinkage Amount

Yixin Shi, Jianfei Liu, Defan Huang, Minzi Xu, Shike Zhai, Wentao Zhang and Ping Jiang *

College of Mechanical and Electrical Engineering, Hunan Agricultural University, Changsha 410128, China

* Correspondence: 1233032@hunau.edu.cn

Abstract: In view of the problems that the fuselage inclines and the driving straightness is difficult to guarantee due to the sinking and sliding of the wheels when the high-clearance plant protection machine is working in the paddy field, this paper takes high-clearance wheels as the research object, based on the paddy field driving environment, establishes a prediction model of the wheel subsidence through derivation, and explores the influence of different wheel parameters on the subsidence characteristics through experiments, so as to improve the chassis trafficability. At the same time, using the test data under different wheel parameters, the prediction model of the settlement of the working chassis with high clearance is correspondingly modified. Finally, the paddy field trafficability of the working chassis is compared and analyzed based on different tire parameters. The results show that when the wheel slip rate is 0.5, the traction force of the solid tire is 37% higher than that of the pneumatic tire; when the height of the wheel spike increases, the traction force increases, and the settlement decreases obviously; proper increase of the wheel diameter can improve the passing performance of the chassis; with the increase of the tire width, the angle of soil penetration decreases while the tire is driving, and the angle of the slope climbing increases; and when the load changes, the driving coefficient is proportional to the traction coefficient, and the tire resistance coefficient is inversely proportional to the traction coefficient. Through the research on the settlement mechanism of the high-clearance operation chassis and the analysis of the paddy field trafficability, the stability of the high-clearance plant protection machine in the paddy field has been improved, providing a platform and guarantee for subsequent precision operation.



Citation: Shi, Y.; Liu, J.; Huang, D.; Xu, M.; Zhai, S.; Zhang, W.; Jiang, P. Prediction and Experimental Study of Tire Slip Rate Based on Chassis Sinkage Amount. *Agriculture* **2023**, *13*, 665. <https://doi.org/10.3390/agriculture13030665>

Academic Editor: Massimo Cecchini

Received: 16 February 2023

Revised: 2 March 2023

Accepted: 12 March 2023

Published: 13 March 2023



Copyright: © 2023 by the authors. Licensee MDPI, Basel, Switzerland. This article is an open access article distributed under the terms and conditions of the Creative Commons Attribution (CC BY) license (<https://creativecommons.org/licenses/by/4.0/>).

Keywords: wheel–ground interaction; sink mechanism; slip rate; sink volume; hook traction

1. Introduction

The prediction of the sinkage and slip rate of agricultural machinery tires is aimed at allowing the optimization of the traction performance and passing performance of vehicles by enabling the appropriate adjustment of the vehicle tire parameters for soil conditions within different operating environments so that the vehicle can maintain good passing performance when moving in the field [1]. At present, there are sufficient theoretical references on the interaction between tires and soil: Baker derived a new stress–strain formula for soil shear properties and bearing properties; Janosi, Z. et al. proposed an “asymptotic linear” correction formula for the soil shear properties derived by Baker [2,3]; Perumpral, J.V. et al. analyzed, for the first time, the deformation and stress distribution of soil under tractor wheels using linear and nonlinear elasticity problem finite element solutions [4,5]; Gerhart, G. et al. studied the driving characteristics of tracked and wheeled vehicles of different sizes and masses under different conditions using Baker’s ground mechanics model [6]; Yoshida, K. et al. performed a simulation of lunar vehicle dynamics based on a rotation rate traction model [7]; and Lyasko, M. et al. investigated a method for predicting vehicle driving resistance considering the sink and slip of a track plate. Some algorithms based on deep learning can enlighten the development of intelligent agricultural machinery [8,9]; Ding, L. et al. proposed a technique for identifying soil parameters based

on decoupling analysis of a wheel–soil interaction ground mechanics model [10]; Chen, D. et al. derived a new wheel–ground interaction force model by combining the distribution of wheel–ground contact stresses [11]; Huang, K. et al. established a finite element model of tire–soft ground contact based on tractor traction tests, analyzed the influence of external parameters on tire traction performance, and verified the validity of the simulation [12]; and Wang Zhengyin established a dynamic mechanical prediction model of tire–ground interaction under a high slip rate by analyzing the principle of tire dynamic sink, which provides a mechanical basis for the development of Mars vehicles [13].

On the basis of the research on the settlement of the chassis for the first time, this paper establishes a high-clearance chassis settlement model through a test and comparative analysis of tires with different types, wheel spike height, wheel diameter, wheel width, and other parameters, and verifies its accuracy and applicability through fitting analysis. This paper further explores the influence of tire parameters on vehicle passing ability in the field by analyzing the test results, providing theoretical basis and practical guidance for optimizing vehicle design, and improving field operation efficiency.

2. Materials and Methods

2.1. Test Platform Structure

The structure of the high-ground-clearance operator is shown in Figure 1, which is mainly composed of a power system, hydraulic system, and control system, and the chassis of the whole vehicle adopts a full hydraulic system; therefore, both the wheelbases and the ground clearance can be adjusted by using a hydraulic adjustment device: one wheelbase is adjustable from 1.6 to 2.4 m, and the other wheelbase is adjustable from 2.4 to 2.9 m [14,15]. The whole-vehicle drive mode adopts a combination of a variable pump and variable motor, which can realize 1~10 grades of infinitely adjustable driving speeds. The plant protection machine is equipped with a vehicle-powered chassis that can be retrofitted with a disassembled spray bar spraying device, fertilizer application device, wind pollination, and other field plant protection operation equipment [16,17]. Its overall design parameters are given in Table 1.



Figure 1. Chassis structure diagram: 1—hydraulic system; 2—engine; 3—operating table; 4—outrigger mechanism; 5—wheels; 6—main frame.

When the machine is operating in the field, the machine’s tire parameters have a great influence on the traction performance and driving performance of the whole machine when driving. Therefore, we focused on the tires of the high-ground-clearance plant protection machine and conducted field tests by adjusting different time parameters to compare and study the interrelationship between time parameters and skid and sink characteristics.

Table 1. Basic technical parameters of overall design.

Form	Unit	Description	Form	Unit	Description
Rated power of engine	Kw/Number of cylinders	55/4	Running speed	Km/h	Continuously variable speed
Rated engine speed	r/min	2600	Traveling system	/	Hydraulic 4WD
Dimension	m	2.2 × 5 × 3	Wheelbase	m	2.4–2.9
Wheelbase	m	1.6–2.4	braking system	/	Hydraulic brake
Ground clearance	m	1.1–1.5	Full load mass	Kg	2200

2.2. Tire Sinkhole Analysis and Model Prediction

By analyzing the force situation of the wheels of the high-ground-clearance plant protection operation vehicle when driving in the field [18–20], a wheel force analysis diagram was drawn, as shown in Figure 2. Based on the analysis of the actual situation during the field test, it was found that the sinkage of the wheels when the vehicle was being driven in the field comprised compaction sinkage and slip sinkage. When moving in the paddy field, due to the high soil viscosity and poor soil environment, the wheels slip very easily, and the slip increases the amount of tire slip and sink; that is, the amount of tire slip and sink increases with an increase in slip rate, and the two show a positive relationship. In this study, different tires of the high-ground-clearance operation chassis were tested to study the effects of different time parameters on the slip-rotation characteristics and related sinkage, and a slip-rotation characteristic motion model of the chassis was constructed based on the related characteristics.

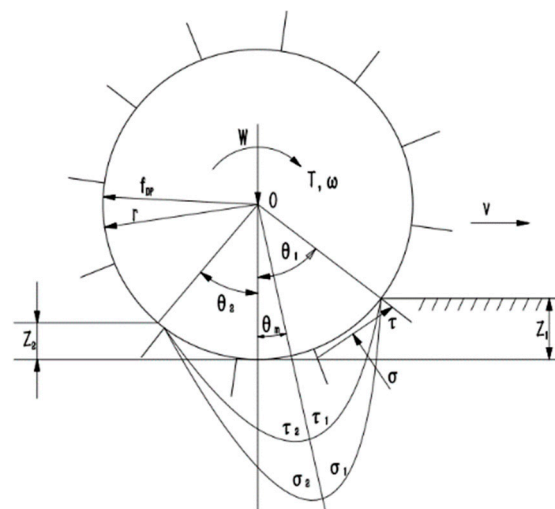


Figure 2. High-ground-clearance operation chassis wheel force analysis diagram. Note: R: radius; ω : angular velocity; v : forward velocity; θ_1 : angle of incidence; θ_2 : angle of departure; θ : angle of action; Z_1 : θ_m : maximum stress angle; maximum sinkage; Z_2 : backfill sinkage; σ : positive stress; τ : shear stress; W : vertical load; f_{DP} : forward resistance; T : driving moment.

According to Figure 2, it can be seen that W and f_{DP} represent the chassis load distribution to the wheels. There is the ground support force and resistance with the corresponding load in an equilibrium of force. Through the analysis of the vehicle’s tire slip, the wheel slip rate can be found—that is, the error between the actual speed of the wheel and the theoretical speed. That is,

$$s = \frac{r\omega - v}{r\omega} \quad (r\omega \geq v, 0 \leq s \leq 1) \tag{1}$$

$$s = \frac{r\omega - v}{v} \quad (r\omega \leq v, 0 \leq s < 1) \tag{2}$$

Here, $s > 0$ indicates that there is slip rotation of the wheel at this time; $s = 0$ indicates pure rolling; and $s < 0$ indicates wheel slip.

To establish a coordinate system with the wheel rotation center, as shown in Figure 3, the wheel forward direction is defined as the x direction, lateral direction as the y direction, and vertical support direction as the z direction; the ground acts as a normal supporting reaction force on the wheel; the wheel adhesion force and shear force on the soil combine to generate a moment of resistance (MR), and through that moment, balance decomposition produces the driving force of the wheel; the amount of sagging in the wheel's driving process comprises the support performance of the soil and the wheel's shear effect together, at the same time—due to the shear force and sagging support force—generating the driving resistance and driving force of the high-ground-clearance operation chassis' FDP [21]. Analysis of the wheel in the driving process mainly considers the role of forces and moments to establish the following equilibrium equations, that is, the chassis' performance mechanics model:

$$\begin{cases} F_N = F_{wz} = F_N(P_S, P_T, P_W, P_R) \\ F_{DP} = F_{wx} = F_{DP}(P_S, P_T, P_W, P_R) \\ F_S = F_{wy} = F_S(P_S, P_T, P_W, P_R) \\ M_O = M_{wx} = F_S(P_S, P_T, P_W, P_R) \\ M_R = -M_{wy} = M_R(P_S, P_T, P_W, P_R) \\ M_S = M_{wz} = M_S(P_S, P_T, P_W, P_R) \end{cases} \quad (3)$$

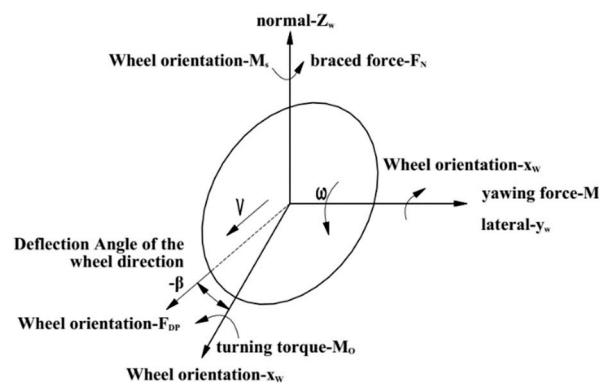


Figure 3. Wheel force diagram. Note: F_{DP} : driving force; M_R : driving resistance moment; F_S : lateral force; F_N : ground support force; M_O : transverse swing moment; M_S : overturning moment.

After drawing a schematic diagram of the tire slip and sink and analyzing Figure 4 to determine the slip and sink characteristics of the tire when driving, we can set the initial contact angle between the tire and the soil as θ_a , the rotation angle of the tire in the time as θ_c , and the slip amount as $\Delta \times 3$. We can then obtain

$$\theta_c = \omega t_c \quad (4)$$

$$r\theta_a = \Delta x_3 = r\omega t_c \cdot (1 - s) \quad (5)$$

$$\frac{1}{2} [(r + h)^2 - r^2] \theta_a = \frac{1}{2} [(r + h')^2 - r^2] \theta_c \quad (6)$$

According to Equations (4)–(6), we obtain

$$\frac{\theta_a}{\theta_c} = 1 - s = \frac{h'[1 + h'/(2r)]}{h[1 + h/(2r)]} \approx \frac{h'}{h} \quad (7)$$

That is, the amount of slip and sinkage due to tire tread shear of soil is

$$\Delta z_3 = h - h' \approx hs \quad (8)$$

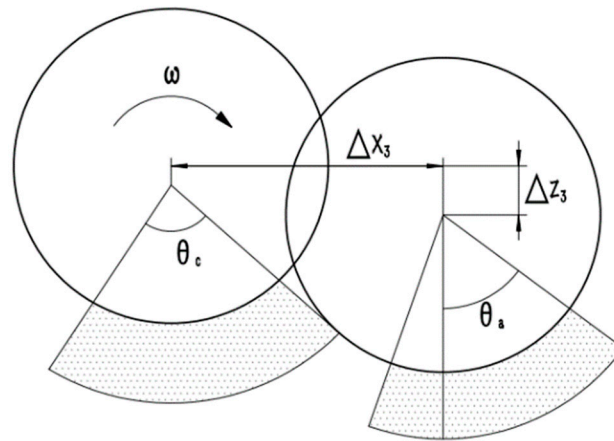


Figure 4. Tire skidding driving diagram. Note: θ_a : Initial contact angle between tire and soil; ΔX_3 : slip travel distance; ΔZ_3 : slip settlement due to tire pattern shearing soil; θ_c : Tire rotation angle; ω : Tire angular speed.

According to Figure 4, the actual tire sinkage can be obtained:

$$z = z_0 + \Delta z_1 + \Delta z_2 + hs - \Delta z_4 \tag{9}$$

According to the test situation, it is concluded that, when the high-ground-clearance chassis is driving in the paddy field, the slip rate is proportional to the amount of sinkage; that is, after the wheel skids in the paddy field, with an increase in slip rate, the amount of wheel sinkage will increase. The tire slip and sink and the paddy field soil’s longitudinal, lateral, and tire tread shear force—as well as other factors—are related; therefore, the study of the tire slip in the paddy field needs to consider a variety of factors.

Based on the literature related to the wheel–ground interaction [22], the wheel hook traction force based on stress distribution is derived as

$$F_P = \frac{bD}{2} \int_0^{\theta_1} [\tau(\theta) \cos \theta - \sigma(\theta) \sin \theta] d\theta \tag{10}$$

The vertical load on the wheels travelling in the field is

$$W = \frac{bD}{2} \int_0^{\theta_1} [\tau(\theta) \sin \theta + \sigma(\theta) \cos \theta] d\theta \tag{11}$$

and according to [23], the relationship between the soil cohesion and internal friction angle can be obtained as

$$\tau = c + \sigma \tan \varphi \tag{12}$$

To establish the functional relationship between the hook traction FP , driving torque T , load W , and sinkage Z , Equations (2)–(10) are first linearized. Let θ_m be the maximum positive stress σ_{\max} and the maximum shear stress τ_{\max} at the bottom surface of the wheel in the contact range.

When $0 \leq \theta \leq \theta_m$, it is found that

$$\sigma_1(\theta) = \frac{2\theta}{\theta_1} \sigma_{\max} \tag{13}$$

$$\tau_1(\theta) = \frac{2\theta}{\theta_1} \tau_{\max} \tag{14}$$

When $\theta_m \leq \theta \leq \theta_1$, it is found that

$$\sigma_2(\theta) = \frac{2(\theta_1 - \theta)}{\theta_1} \sigma_{\max} \tag{15}$$

$$\tau_2(\theta) = \frac{2(\theta_1 - \theta)}{\theta_1} \tau_{\max} \tag{16}$$

Bringing (13), (14), (15), and (16) into (10) gives

$$F_p = \frac{\left(2 \cos \frac{\theta_1}{2} - \cos \theta_1 - 1\right)^2 + \left(2 \sin \frac{\theta_1}{2} - \sin \theta_1\right)^2}{2 \cos \frac{\theta_1}{2} - \cos \theta_1 - 1} \times \frac{8T}{\theta_1^2 D} - \frac{2 \sin \frac{\theta_1}{2} - \sin \theta_1}{2 \cos \frac{\theta_1}{2} - \cos \theta_1 - 1} W \tag{17}$$

Taking into account the limit conditions of high-clearance chassis driving in the field, (17) can be simplified as

$$F_p = \left(1 + \frac{\theta_1^2}{4}\right) \frac{2T}{D} - \frac{\theta_1}{2} W \approx \frac{2T}{D} - \frac{\theta_1}{2} W \tag{18}$$

Moreover, based on $\theta_1 \approx \frac{4z}{D}$ [24–26], simplifying Equation (17) yields the sinkhole prediction model for hook traction and load as

$$\frac{F_p}{W} = \frac{2T}{DW} - \frac{2z}{D} \tag{19}$$

It is a functional relationship based on the four variables of hook traction (F_p), driving torque (T), load (W) and settlement (Z), which can be used as the settlement prediction model of the hook traction and load of the high-clearance chassis. The prediction accuracy can be further improved by applying a one-line correction to (19) [27] and bringing the experimental data into the transformation yields.

$$\frac{F_p}{W} = \frac{T}{DW} + \frac{z}{D} + C_3 \tag{20}$$

C_3 is the correction coefficient that varies the most with the load. From the test data, it is found that C_3 is proportional to the actual load on the chassis, i.e.,

$$C_3 = -1.062 \times 10^{-6} w^2 + 2.2^6 \times 10^{-3} w - 1.467 \tag{21}$$

Based on the traction model of the high-ground-clearance operation chassis obtained by Equation (20), the effect of different tire parameters on the slip rate and sinkage amount was investigated by designing field tests and installing different tires on the same chassis for the study, with solid and pneumatic tires, wheel spur heights of 40 mm and 50 mm, diameters of 900 mm and 1100 m, and widths of 100 m and 140 m, respectively. The combination comparison test was conducted by adding correction coefficients of (0.5, 0, k selected as 14.2) and refitting the original sinkage model data for the correlation between the sinkage index and load.

2.3. Field Trials

The test instruments included the following: a ZJ-1A strain-controlled manual straight shear soil firmness tester SpectrumSC900 (USA), a soil moisture tester TDR-300 (UK), Revo 704-wheel tractor (CHN), a Beidou locator, push–pull tester (HP-50k), a Reynolds hydraulic tester CHPM480-05-0C (CHN), and a special pressure and flow sensor for the tester, oil pipe fitting, leather ruler, etc.

The test paddy field was an on-campus test field, which was treated with shaking and turning the billet before the test, and then, the soil was sampled to test its parameters such as shear strength, moisture, and firmness [28,29]. The cohesion (c) of the soil was measured to be 4.14 kPa, the angle of internal friction (φ) of the soil was 10° according to the straight shear test and the plate bearing test, and the weather that day was recorded as cloudy and with a temperature of 17 °C, as shown in Figure 5.



Figure 5. Field test of high-ground-clearance operating chassis.

According to the current agricultural machinery production test methods [30,31], a straight-line area of 50 m in length was selected as a test plot within the paddy field; the high-ground-clearance planters were pulled by a Reeva tractor (a tensiometer was added in the middle of the two vehicles to measure the traction force of the planters, and the selected driving route was staggered with the vehicle track during the billet-turning operation); and pressure sensors and flow sensors were added to the import and export of the planters' hydraulic motors Danfoss MS02 axial piston motor (DK). A flow sensor is used to measure the real-time flow of motor, and then calculate the wheel speed based on the flow–speed curve of the hydraulic motor. The pressure sensor collected the differential pressure (ΔP) of the hydraulic motor to calculate the driving torque of the wheels, the Beidou locator was used to measure the actual speed of the driving, and the sink depth was measured for every 100 mm on the vehicle track travelled by the planting machine [32,33]. That is, the actual speed of the chassis is measured by the Beidou positioning module, and the theoretical speed is calculated by the hydraulic motor speed of the chassis itself, so that the slip rate of the working chassis during traction and dragging can be obtained. Based on this, different tires were replaced for the test and the measured data were recorded.

3. Results

First of all, the sizes of the traction force and traction coefficient were compared and analyzed when solid rubber tires and pneumatic rubber tires were installed with the same parameters, respectively; the appearance of the tires is shown in Figure 6. The traction forces obtained from the two sets of tests were recorded separately, the wheel sinkage was measured, and the test data were processed to obtain the results shown in Figure 7.



Figure 6. Solid rubber tires (left) and pneumatic rubber tires (right).

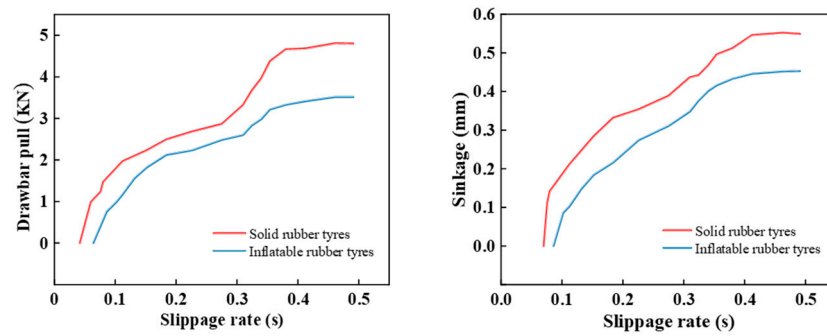


Figure 7. Comparison of the performance of solid and pneumatic tires.

Analysis of Figure 7 shows that, under the same traction conditions, the slip rate of pneumatic rubber tires is greater than that of solid rubber tires, and pneumatic tires are prone to breakage and other conditions in the complex farmland environment, so the next step is to take solid rubber tires as the basis of the experiment and continue the comparative test analysis of structural parameters such as the wheel spurs, wheel diameter, and wheel width of solid tires.

Solid rubber tires were selected to continue the comparative test analysis for tires of different wheel spur heights. In the case of other external environmental factors remaining unchanged, the outer rim of steel tires was directly added to welded angle iron to enable comparisons for different wheel spur heights for solid steel tires. The wheel spur height, h , was chosen to be 40 mm and 50 mm, respectively; the vehicle sinkage, driving torque, and hook traction were measured and recorded; and the predicted curves of the traction, driving force, and tire sinkage under different spur heights were obtained after the test data and line fitting calculation, as shown in Figure 8.

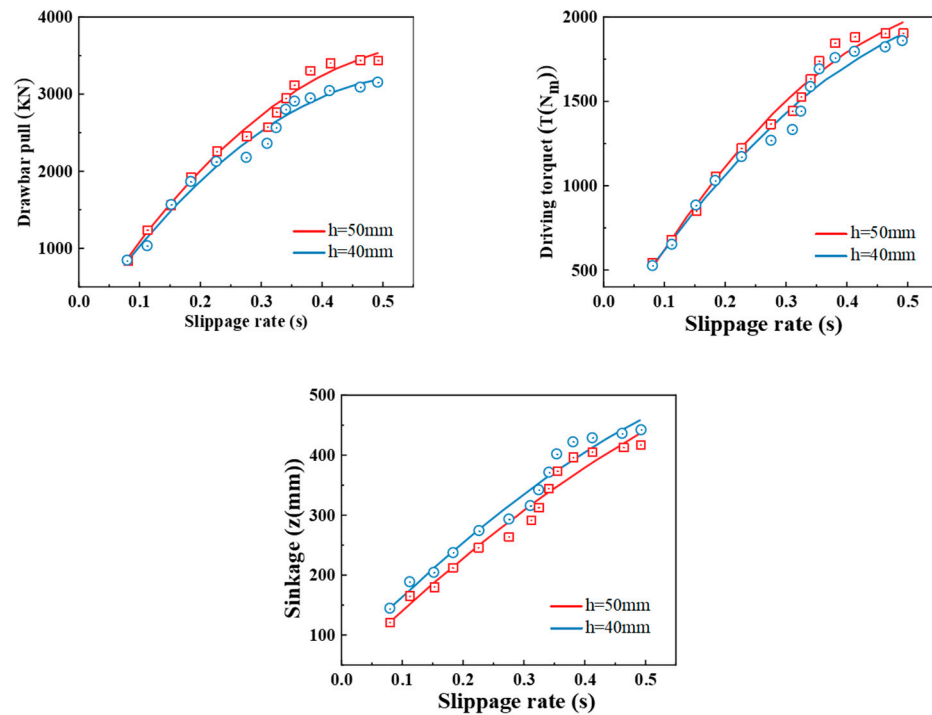


Figure 8. Comparative analysis of the passing performance of different wheel spur heights.

Analysis of Figure 8 shows that the wheel spur height is proportional to the hook traction and driving torque, and inversely proportional to the amount of sinkage. To improve the vehicle's performance within the paddy field, the effects of other parameters on wheel performance were explored based on tires with higher wheel spurs.

To investigate the influence of wheel diameter and wheel width on the performance of the whole machine, the experimental design was installed on the chassis of the high-ground-clearance operator, with wheel diameters of 900 mm (where $n = 0.505 + 2.225 s$) and 1100 mm (where $n = 0.574 + 2.043 s$), respectively, for field tests, and the data obtained were fitted and calculated to obtain the sinkage volume-fitting prediction data formed based on the slip rate. The sinkage volume law curve based on the change in slip rate is shown in Figure 9. It can be seen from the linearity of the fitted curve that the predicted relationship between the fitted slip rate and the sinkage volume is in good agreement with the actual test data, and it can be seen from the data that the fitted curve for the modified sinkage characteristics and the experimental values basically match.

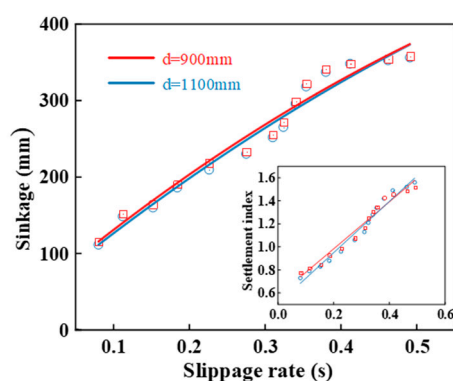


Figure 9. Fitting curve for sink characteristics for wheel diameter 0.9 m and wheel diameter 1.1 m.

Using the aforementioned comparative test method, analysis of the sinkhole model data statistics was carried out for tires with wheel diameters of 900 mm and 1100 mm. The prediction curves obtained after the test data and fitting calculations are shown in Figure 10, and a comparative analysis of the traction characteristics, drive characteristics, and tire sinkhole volume of the high-ground-clearance truck could be performed: when the wheel diameter was changed from 900 mm to 1100 mm, the traction characteristics increased from 3.16 kN to 3.64 kN, with a 15.2% performance improvement; the driving characteristics (hydraulic motor feedback driving torque) increased from 1709 Nm to 1824 Nm, with a 6.7% performance improvement; and the maximum sinkage volume was reduced from 432 mm to 375 mm, with a 13.2% sinkage reduction.

When the tire diameter increases, the amount of sinkage decreases, and there is an overall increase in paddy field trafficability. Therefore, to improve the overall vehicle performance in the paddy field, the traction performance and driving performance can be increased by appropriately selecting tires with a wider wheel diameter to reduce the sinkage, but the selection of tires with too large a wheel diameter will increase the height of the vehicle, making the ground clearance of the chassis too large and, thus, reducing the stability of the vehicle; therefore, the selected wheel diameter should be appropriately increased within a certain range, taking into account the actual situation.

To study the effect of the tire width on the slip rate, tires with wheel diameters of 900 mm and 1100 mm and widths of 100 mm and 140 mm were selected for a combined comparison test under the same external parameters, such as control load, speed, and tire tread pattern. The prediction curves obtained after the line-fitting process for the measured data are shown in Figure 11.

From Figure 11, it can be seen that as the tire width increases, even when the wheel diameter is the same, the soil cutting angle when the tire is moving decreases and the climbing angle subsequently increases. Within the test range, the larger the tire width, the better the performance in paddy fields. Therefore, one can choose to install a larger-width tire to improve the performance of the whole vehicle, but according to the actual operation of the high-ground-clearance planters, to avoid overwhelming the operation. If one chooses to move between the crop rows, the width should be smaller; wider tires may result in

pressure being put on seedlings during driving, and the increased tire width will lead to an increase in the torque of the vehicle when turning, causing a greater burden on the hydraulic steering system of the high-ground-clearance machine. The tire width should be selected based on the maximum crop row spacing and all factors to ensure the stability of the vehicle based on stable driving, light steering, and no pressure on the seedlings.

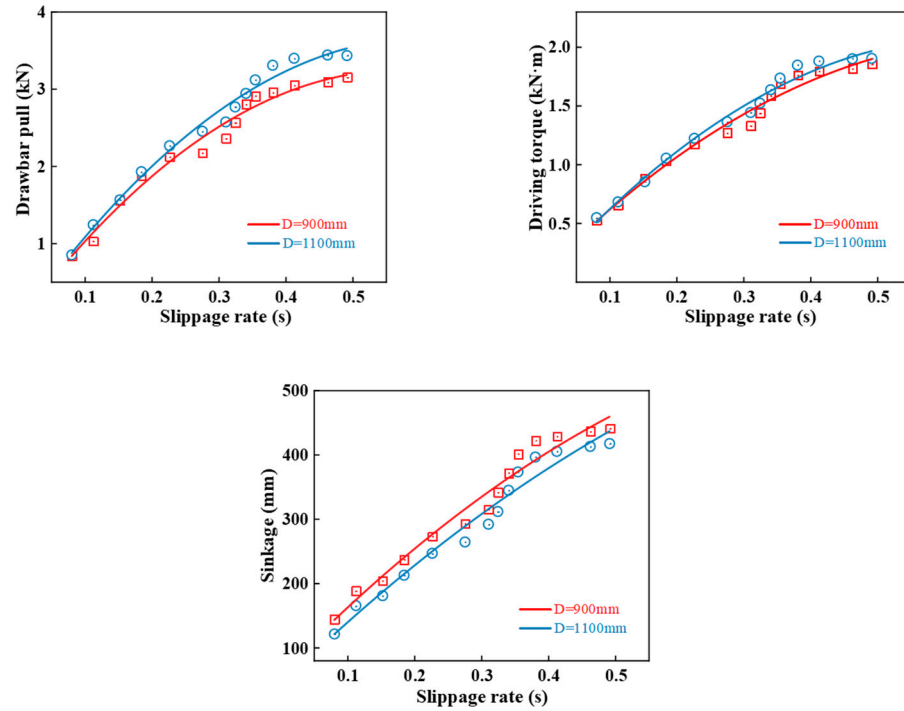


Figure 10. Comparison of passing performance data with different wheel diameters.

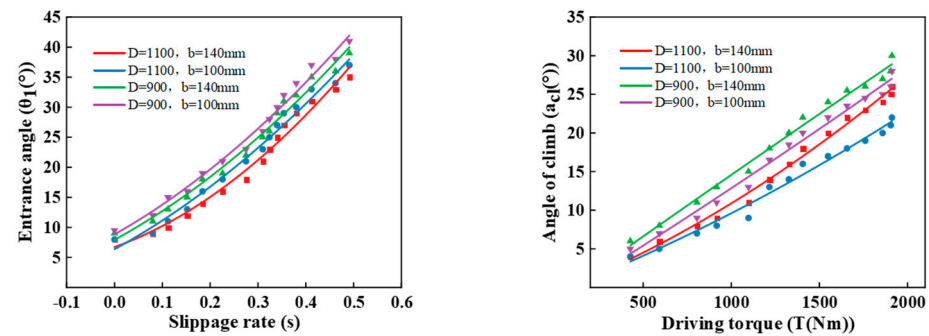


Figure 11. The effect of tire width on passing performance.

Based on the existing test conditions, keeping other parameters unchanged, by adjusting the mass of water in the water tank on the operating vehicle to control the vehicle load, the passing performance of the operating chassis under different load conditions was compared and analyzed, and masses of 8000 N, 9000 N, 1000 N and 1100 N, respectively, were selected to study and analyze the effect of the vehicle load on the wheel slip rate. The test data were calculated by line fitting, as shown in Figure 12, and the predicted curve from the analysis shows that when the load increases, the increased ratio of the wheel sinkage is smaller than the increased ratio of the traction characteristics, and it can be considered that the traction characteristics are more sensitive with the change in load. At the same time, the comparison found that the driving performance of the high-ground-clearance operation chassis is inversely proportional to the load change, and the reason for this finding is that the load increases and the sinkage increases at the same time, causing the chassis to increase its resistance when driving in the paddy field.

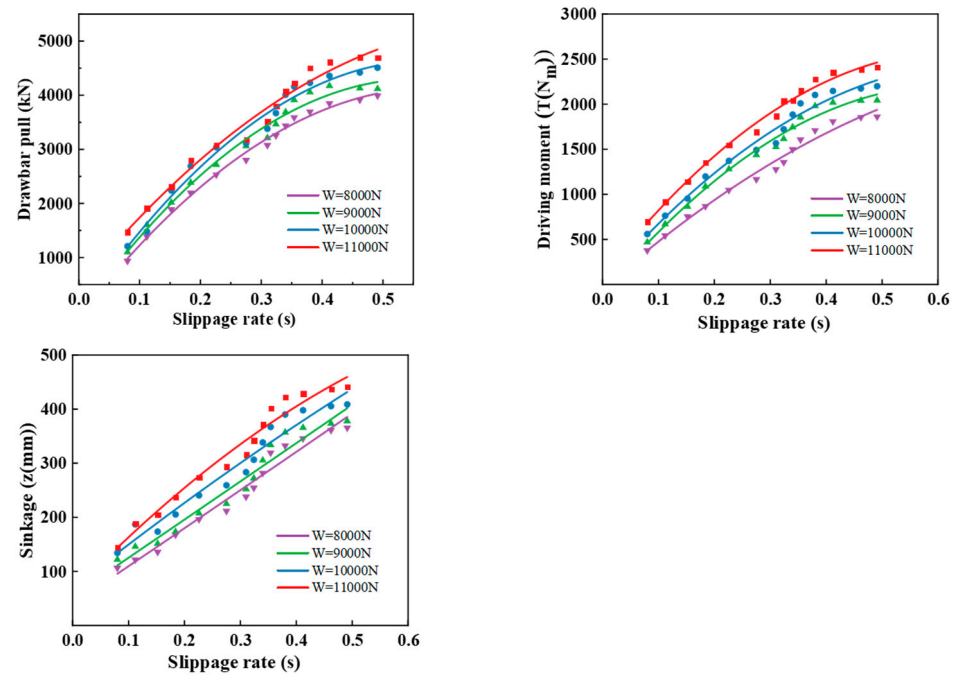


Figure 12. Comparison of passing performance under different load conditions.

By comparing and analyzing the traction characteristics, driving characteristics, and settlement of the chassis with high clearance under different tire parameters, the following conclusions are drawn: the paddy field trafficability of solid rubber tire is better than that of pneumatic rubber tire; the wheel spike height is inversely proportional to the vehicle settlement; with the increase of wheel diameter, the traction characteristics are increased from 3.16 kN to 3.64 kN, and the performance is improved by 15.2%; the driving characteristics were improved from 1709 Nm to 1824 Nm, and the performance was improved by 6.7%; the maximum settlement decreased from 432 mm to 375 mm, and the settlement decreased by 13.2%; when the slip rate is 0.5, and the tire width increases from 0.1 m to 0.14 m, the cutting angle decreases from 34.4 to 30.3; when the load increases and the slip rate is 0.5, the traction force increases from 3.76 kN to 4.13 kN, and the traction characteristics increase by 9.84%; the settlement increased from 369 mm to 402 mm, and the settlement increased by 8.94%; when the load changes, the driving coefficient is proportional to the traction coefficient, and the tire resistance coefficient is inversely proportional to the traction coefficient; and when the slip rate is 0.5, the traction coefficient decreases from 0.57 to 0.45, down by 21%.

4. Conclusions

Based on the paddy field driving environment and taking the high-clearance wheel chassis as the research object, this paper establishes a settlement prediction model. Through comparing and analyzing the traction characteristics, driving characteristics, and settlement of the high-clearance operation chassis under different wheel parameters, the following conclusions are drawn: the paddy field passing performance of solid rubber tire is better than that of pneumatic rubber tire; the height of wheel spike is inversely proportional to the vehicle settlement; and when the load changes, the driving coefficient is proportional to the traction coefficient, and the tire resistance coefficient is inversely proportional to the traction coefficient.

The above conclusions provide theoretical support and experimental demonstration for the settlement prediction and wheel slip of the high-clearance chassis under the paddy field driving environment. At the same time of improving chassis trafficability by estimating wheel subsidence, it provides platform support for the precise spray operation of the high-clearance chassis and leveling of the spray bar. At the same time, based on the subsidence

prediction and slip characteristics of the above models, it can complete real-time correction and calibration of the actual driving speed of the chassis, and achieve accurate control of operating parameters during intelligent and precise plant protection operations.

At the same time, the revised model can be extended to other paddy field wheeled operation chassis in the future, which does not provide a certain method and test reference for the paddy field driving environment.

Author Contributions: Conceptualization, Y.S. and J.L.; methodology, Y.S.; software, Y.S. and J.L.; validation, D.H., M.X., S.Z. and W.Z.; formal analysis, Y.S.; investigation, J.L.; resources, Y.S.; data curation, Y.S.; writing—original draft preparation, Y.S.; writing—review and editing, Y.S., J.L. and P.J.; visualization, Y.S.; supervision, Y.S. and P.J.; project administration, Y.S.; funding acquisition, Y.S. and P.J. All authors have read and agreed to the published version of the manuscript.

Funding: The research has been funded by the Science Research Project of Education Department of Hunan Province (No. 21B0207), the National Key R&D Program Project Subproject (2022YFD2002001) and the Natural Science Foundation of Changsha (No. KQ2208069).

Institutional Review Board Statement: Not applicable.

Data Availability Statement: Not applicable.

Conflicts of Interest: The authors declare no conflict of interest.

References

1. Wang, R. A related study based on vehicle ground mechanics. *Automot. Knowl.* **2022**, *4*, 022.
2. Zhang, K. *Vehicle Terramechanics*; National Defense Industry Press: Beijing, China, 2002. (In Chinese)
3. Yang, S.; Shi, M. *Ground Mechanics and Working Theory of Engineering Machinery*; China Communications Press: Beijing, China, 2010. (In Chinese)
4. Perumpral, J.; Liljedahl, J.; Perloff, W. A numerical method for predicting the stress distribution and soil deformation under a tractor wheel. *J. Terramechanics* **1971**, *8*, 9–22. [[CrossRef](#)]
5. Perumpral, J.; Perloff, J. The Finite Element Method for Predicting Stress Distribution and Soil Deformation under a Tractive Device. *Trans. ASABE* **1971**, *14*, 1184–1188. [[CrossRef](#)]
6. Gerhart, G.; Laughery, S.; Goetz, R. Off-road vehicle locomotion using Bekker's model. In *Unmanned Ground Vehicle Technology II, Proceedings of the SPIE—The International Society for Optical Engineering, Orlando, FL, USA, 24–28 April 2000*; Gerhart, G.R., Gunderson, R.W., Shoemaker, C.M., Eds.; SPIE: Washington, DC, USA, 2000; Volume 4024, pp. 127–136.
7. Yoshida, K.; Hamano, H. Motion dynamics of a rover with slip-based traction model. In Proceedings of the 2002 IEEE International Conference on Robotics and Automation, Washington, DC, USA, 11–15 May 2002.
8. Lyasko, M. Slip sinkage effect in soil–Vehicle mechanics. *J. Terramechanics* **2010**, *47*, 21–31. [[CrossRef](#)]
9. Liu, T.; Ma, Y.; Yang, W.; Ji, W.; Wang, R.; Jiang, P. Spatial-temporal interaction learning based two-stream network for action recognition. *Inf. Sci. Int. J.* **2022**, *606*, 864–876. [[CrossRef](#)]
10. Liang, D.; Haibo, G.; Zongquan, D.; Jicheng, L.; Jianguo, T. Ground mechanics model of lunar wheel-ground interaction based on stress distribution. *J. Mech. Eng.* **2009**, *45*, 49–55.
11. Chen, D.; Hou, L.; Zhu, Q.; Bu, X. Wheel-ground interaction force model considering tire geometry and tire pressure factors and its parameter identification. *J. Mech. Eng.* **2020**, *2*, 10.
12. Huang, K. Numerical Simulation of the Interaction Between Tractor Tires and Soft Ground. Master's Thesis, Jilin University, Changchun, China, 2021.
13. Wang, Z. Experimental and Modeling Study on the Ground Action of High-Slip Sinker Wheels with Planet Wheels. Master's Thesis, Harbin Institute of Technology, Harbin, China, 2020.
14. Shi, Y.; Jiang, P.; Lu, X.; Dong, C.; Hu, W.; Luo, Y. Design and Experiment on Chassis Structure for Highland Gap Field. *J. Agric. Eng.* **2019**, *9*, 72–79.
15. Fujiwara, D.; Iizuka, K.; Asami, D.; Kawamura, T.; Suzuki, S. Study on Traveling Performance for Variable Wheel-Base Robot Using Subsidence Effect. *Int. J. Mech. Eng. Robot. Res.* **2019**, *8*, 233–238. [[CrossRef](#)]
16. Li, Z.; Shi, Y.; Jiang, P.; Hu, W.; Lin, W. Design and experimental research of high clearance universal operation chassis. *Food Mach.* **2018**, *34*, 100–105.
17. Shu, X.; Jiang, P.; Hu, W.; Shi, Y.; Lin, W.; Dong, C. Design and test of the chassis leveling system for the high ground gap plant protection machine. *J. Hunan Agric. Univ.* **2019**, *45*, 321–326.
18. Yu, B.; Niu, R.; Hua, C. Ground vehicle mobility assessment methods and applications. *J. Jilin Univ. Eng. Ed.* **2022**, *52*, 1229–1244.
19. Srikonda, S.; Norris, W.R.; Nottage, D.; Soylemezoglu, A. Deep Reinforcement Learning for Autonomous Dynamic Skid Steer Vehicle Trajectory Tracking. *Robotics* **2022**, *11*, 95. [[CrossRef](#)]

20. Han, Y.; Lu, Y.; Chen, N.; Wang, H. Research on the Identification of Tyre-Road Peak Friction Coefficient under Full Slip Rate Range Based on Normalized Tyre Model. *Actuators* **2022**, *11*, 59. [[CrossRef](#)]
21. Ding, L. A Ground Mechanics Model of Lunar/Planetary Wheel-Ground Interaction and Its Application. Master's Thesis, Harbin Institute of Technology, Harbin, China, 2011.
22. Ding, L.; Gao, H.; Deng, Z.; Liu, J.; Tao, J. Terramechanics model for wheel-terrain interaction of lunar rover based on stress distribution. *Chin. J. Mech. Eng.* **2009**, *45*, 49–55. [[CrossRef](#)]
23. Ding, L.; Xiao, J.; Zong, W.; Liu, D.; Yang, X.; Zou, M. Drawbar pull model of planetary rover associated with subsidence. *Trans. Chin. Soc. Agric. Mach.* **2014**, *45*, 37–42.
24. Gao, H.; Guo, J.; Liang, D.; Nan, L.; Zhen, L.; Liu, G.; Deng, Z. Longitudinal skid model for wheels of planetary exploration rovers based on terramechanics. *J. Terramechanics* **2013**, *50*, 327–343. [[CrossRef](#)]
25. Jayakumar, P.; Melanz, D.; Maclennan, J.; Gorsich, D.; Senatore, C.; Iagnemma, K. Scalability of classical terramechanics models for lightweight vehicle applications incorporating stochastic modeling and uncertainty propagation. *J. Terramechanics* **2014**, *54*, 37–57. [[CrossRef](#)]
26. Jiang, L.; Liu, X.; Jiang, Y. Research on lunar rover wheel-soil interaction model. *Veh. Power Technol.* **2013**, *31*, 1–6.
27. Jin, D.; Li, J.; Dang, Z.; Chen, B.; Zou, M. Study on model for sinkage of lunar rover wheel under slip. *Acta Aeronaut. Astronaut. Sin.* **2013**, *34*, 1215–1221.
28. Liu, Y. Soil Traffichability Study Based on Mechanical Properties of Paddy Soil. Ph.D. Dissertation, Nanjing Agricultural University, Nanjing, China, 2014.
29. Li, W.; Li, J. Vehicle ground mechanics experiments. *Automot. Knowl.* **2022**, *4*, 022.
30. Wang, W.; Xu, X.; Xu, H.; Wang, L. Tractive performance prediction for wheeled unmanned vehicles based on dynamics and discrete element method. *Proc. Inst. Mech. Eng. D J. Automob. Eng.* **2021**, *235*, 1643–1659. [[CrossRef](#)]
31. Mousavi, H.; Sandu, C. Experimental Study of Tread Rubber Compound Effects on Tire Performance on Ice. *SAE Int. J. Commer. Veh.* **2020**, *13*, 99–101. [[CrossRef](#)]
32. Watanabe, T.; Iizuka, K. Study on connection between shape of wheel and resistance force from ground for small wheel typed rovers. *IOP Conf. Ser. Mater. Sci. Eng.* **2020**, *904*, 12006–12007. [[CrossRef](#)]
33. Els, S.P.; Botha, T.R. Digital image correlation techniques for measuring tyre-road interface parameters: Part 2-Longitudinal tyre slip ratio measurement. *J. Terramech.* **2015**, *61*, 101–112. [[CrossRef](#)]

Disclaimer/Publisher's Note: The statements, opinions and data contained in all publications are solely those of the individual author(s) and contributor(s) and not of MDPI and/or the editor(s). MDPI and/or the editor(s) disclaim responsibility for any injury to people or property resulting from any ideas, methods, instructions or products referred to in the content.